Electronic Supplementary Information

Rational design of multi-shelled CoO/Co_9S_8 hollow microspheres for high-performance hybrid supercapacitors

Yaping Wang,[a,b] Ting Zhu,*[a] Yifang Zhang,[a] Xiangzhong Kong,[a] Shuquan Liang,[a] Guozhong Cao[c] and Anqiang Pan,*[a]

[a] School of Materials science and Engineering, Central South University, Changsha, 410083, Hunan, China

[b] Light Alloy Research Institute, Central South University, Changsha, 410083, Hunan, China

[c] Department of Materials Science and Engineering, University of Washington, Seattle, WA, 98195, USA.

* Corresponding authors: pananqiang@csu.edu.cn; Zhut0002@csu.edu.cn

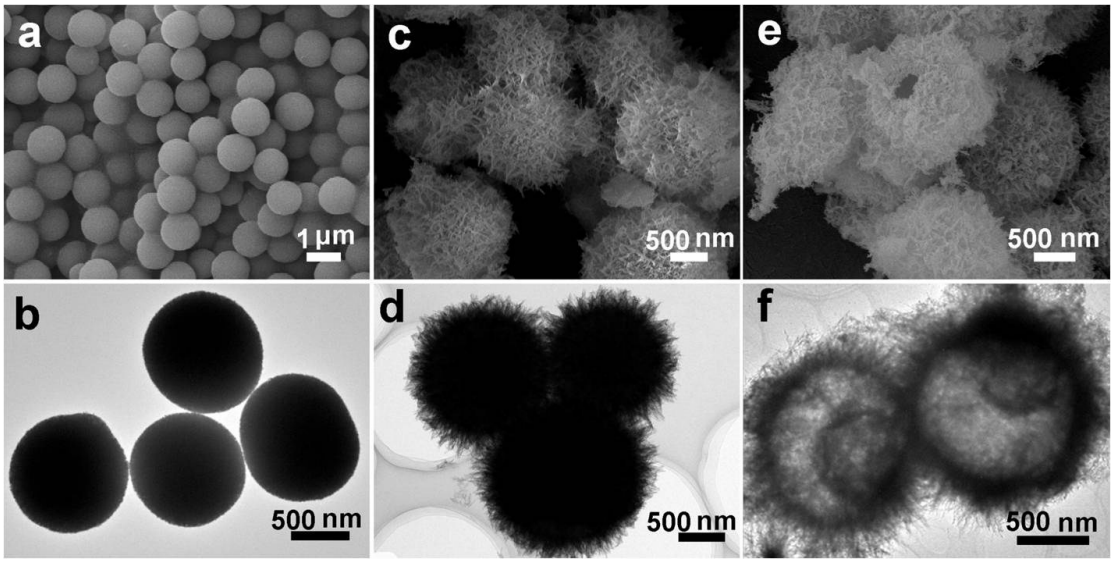

Fig. S1. SEM images(a-e) and TEM (b-f) images of the carbon spheres (a and b), the core-shelled CS@$Co_2CO_3(OH)_2$ (c and d) and the multi-shelled Co_3O_4 hollow spheres (e and f), respectively .

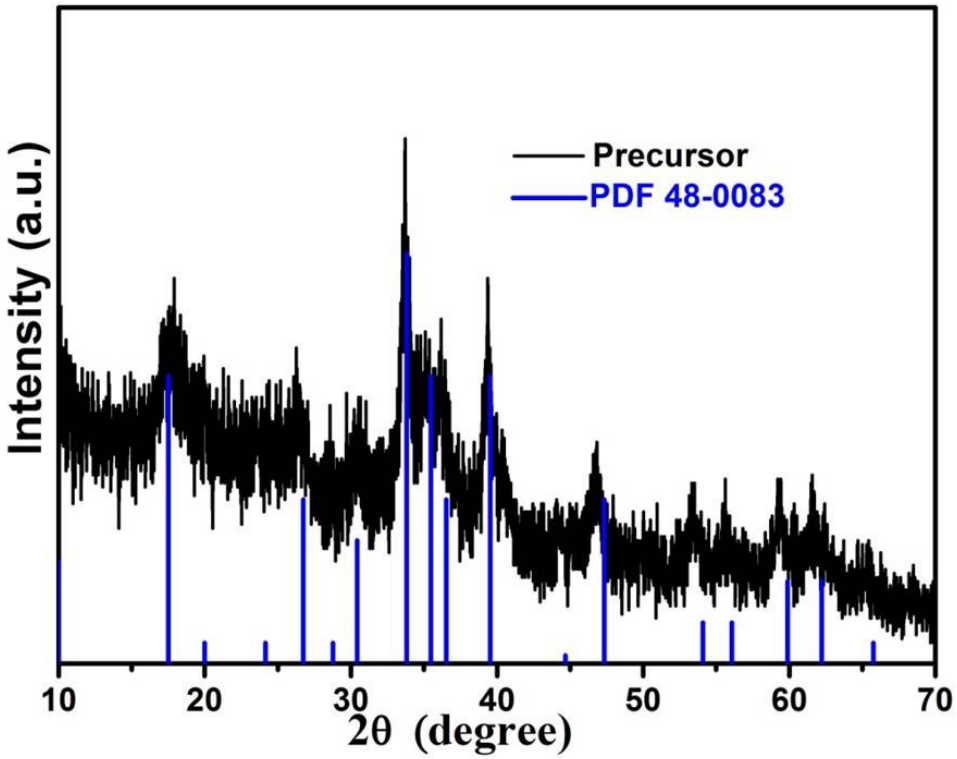

Fig. S2. The XRD patterns of the CS@$Co_2CO_3(OH)_2$ precursor.

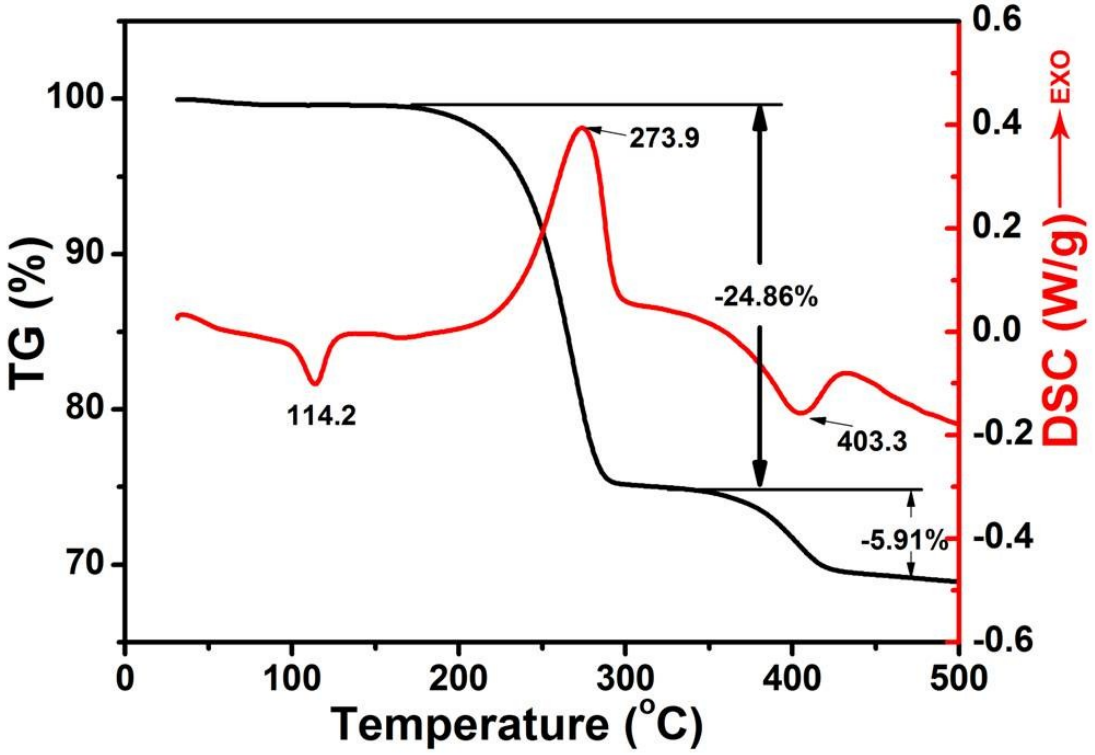

Fig. S3. TG and DSC curves of the mixture of Co_3O_4 and S powder.

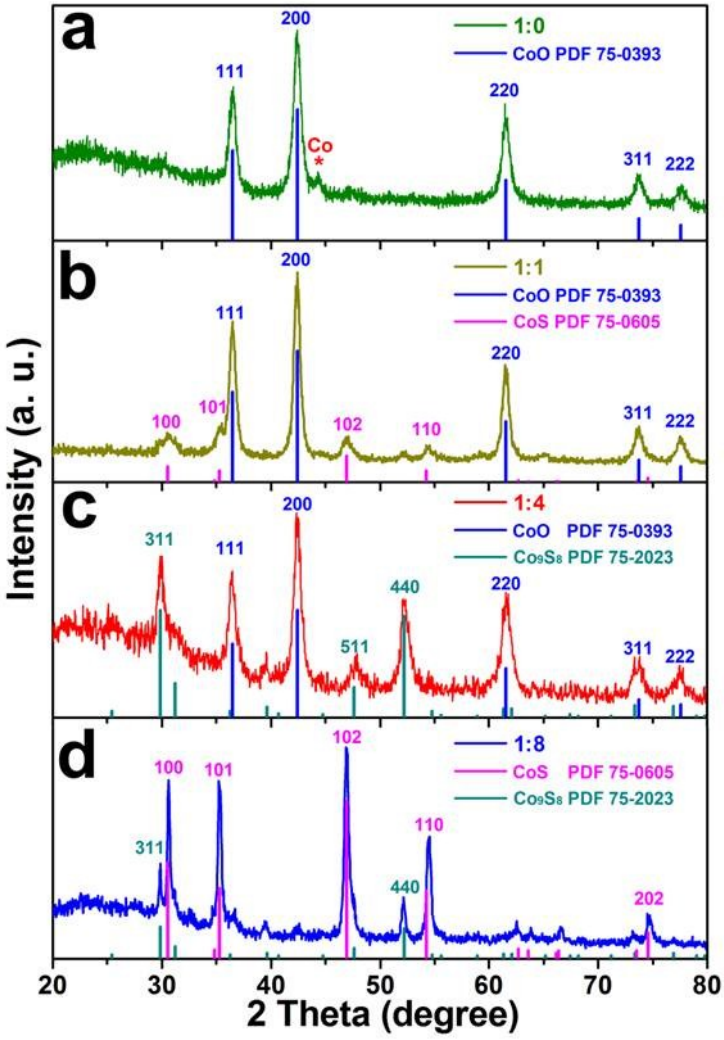

Fig. S4. XRD patterns of the multi-shelled cobalt oxides/sulfides composite hollow spheres.

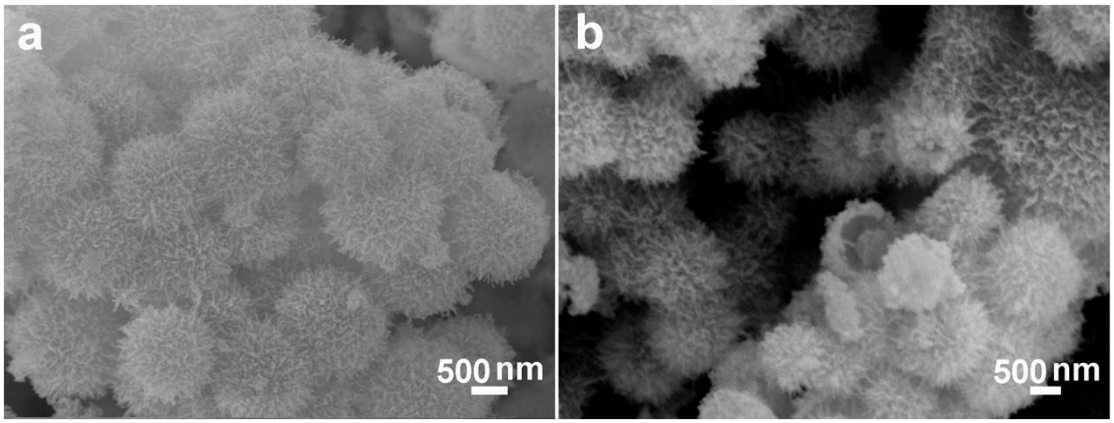

Fig. S5. SEM images of the multi-shelled CoO/CoS (a) and the CoS/Co_9S_8 (b) hollow spheres.

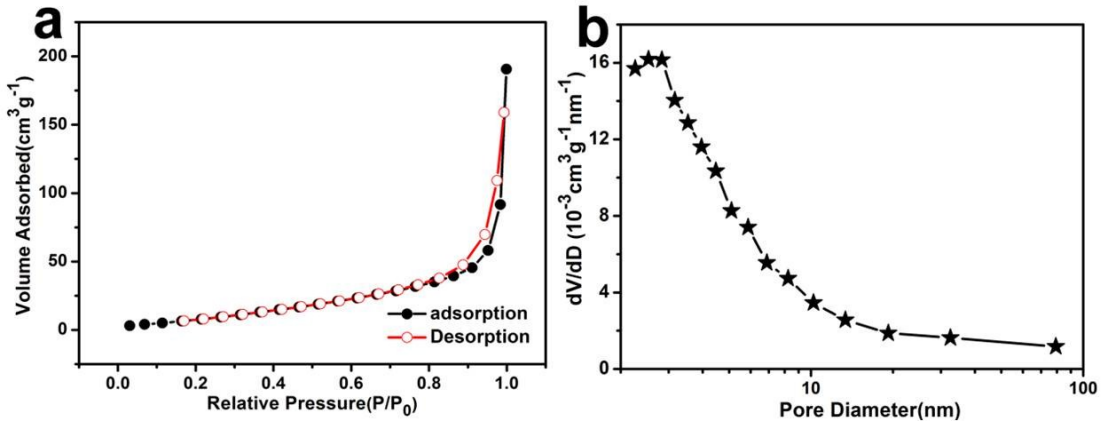

Fig. S6. Nitrogen adsorption-desorption isotherms (a) and pore size distribution (b) of the multi-shelled CoO /Co_9S_8 composite hollow spheres.

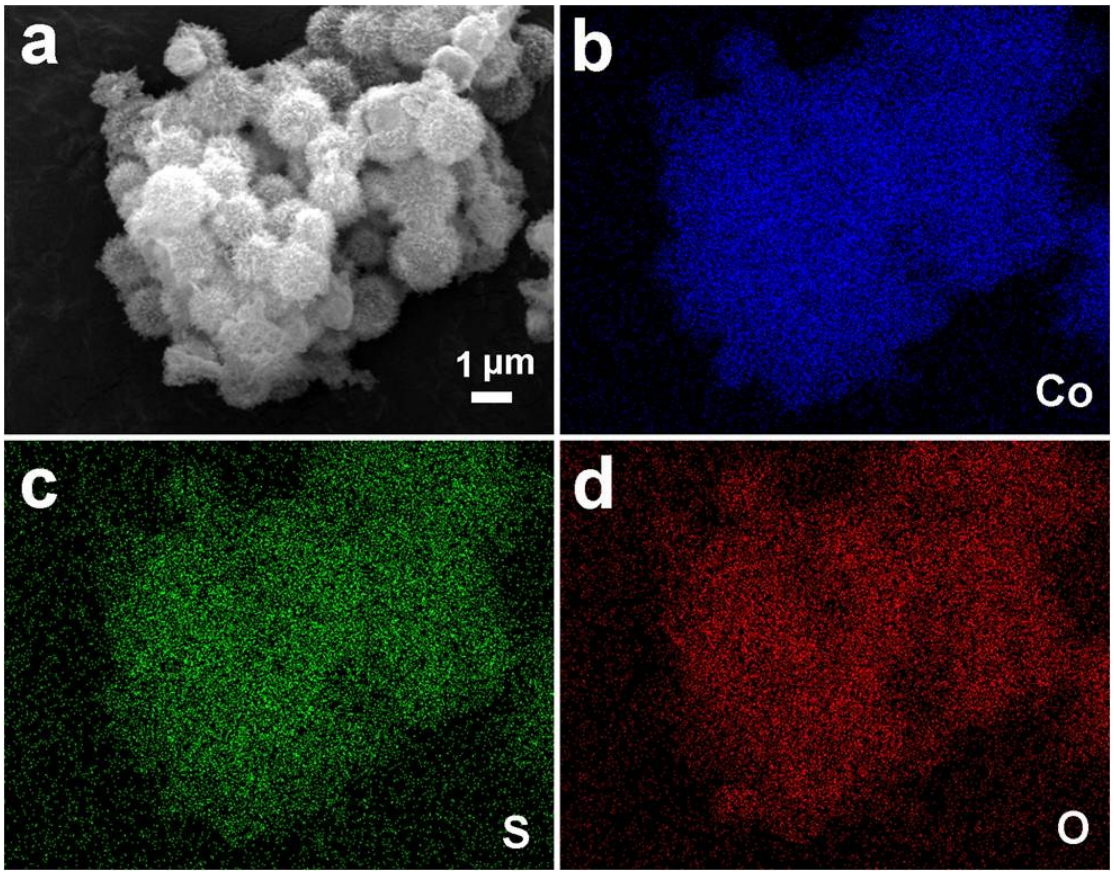

Fig. S7. The elemental mapping results from SEM of CoO / Co_9S_8 microspheres.

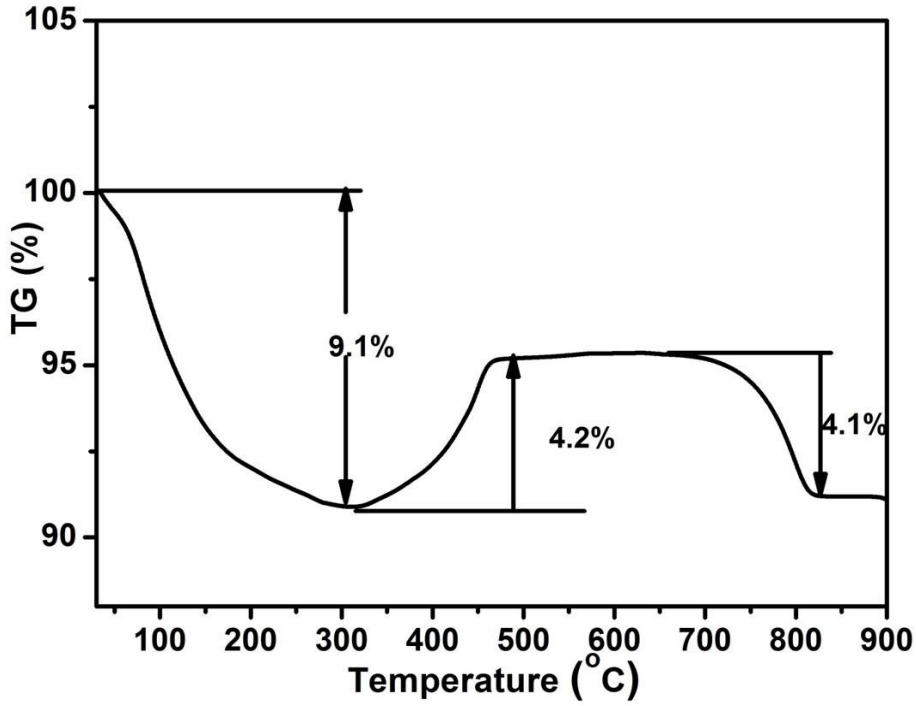

Fig. S8. TG curves of the CoO/ Co_9S_8 powders measured in air with a ramp rate of 10 $^{o}C\ min^{-1}$.

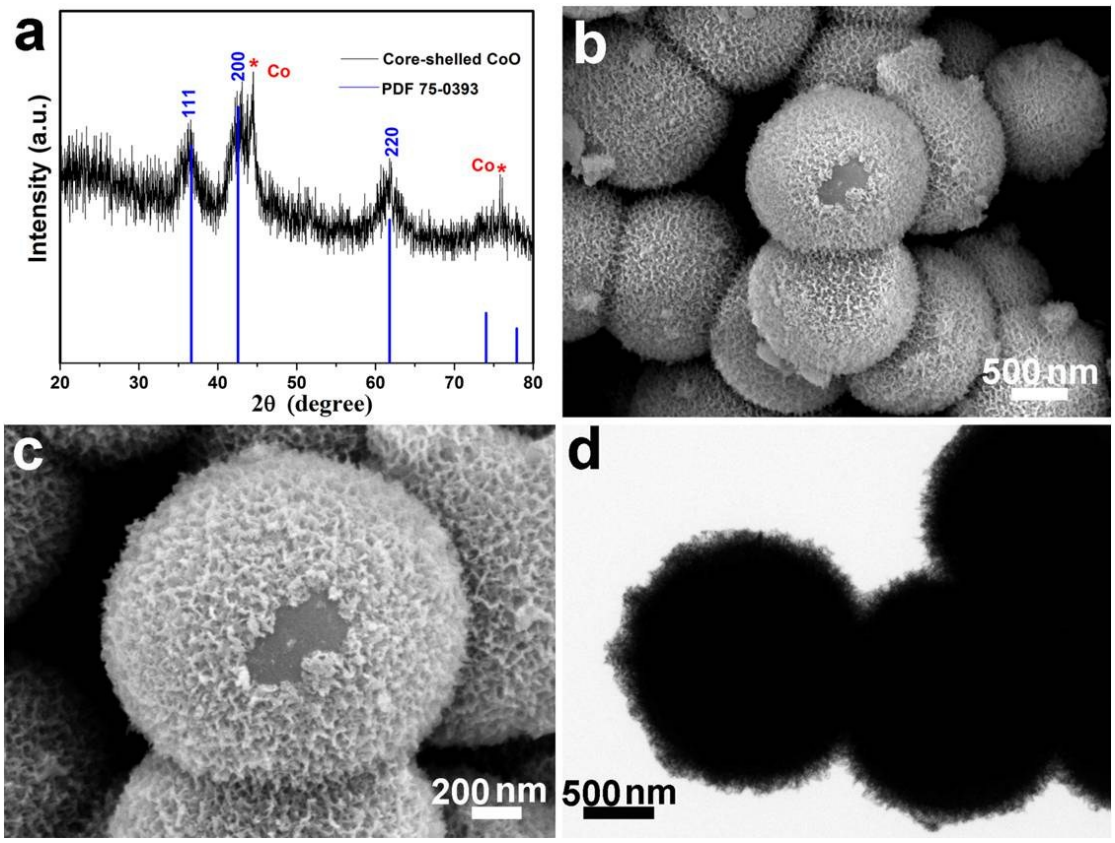

Fig. S9. XRD pattern (a), SEM images (b and c) and TEM image (d) of the core-shelled CS@CoO microspheres.

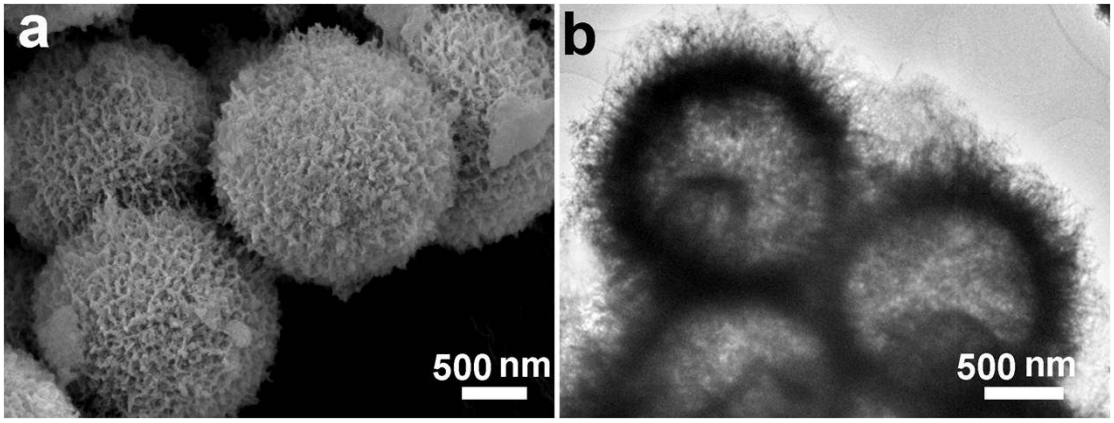

Fig. S10. SEM image (a) and TEM image (b) of the multi-shelled CoO hollow spheres.

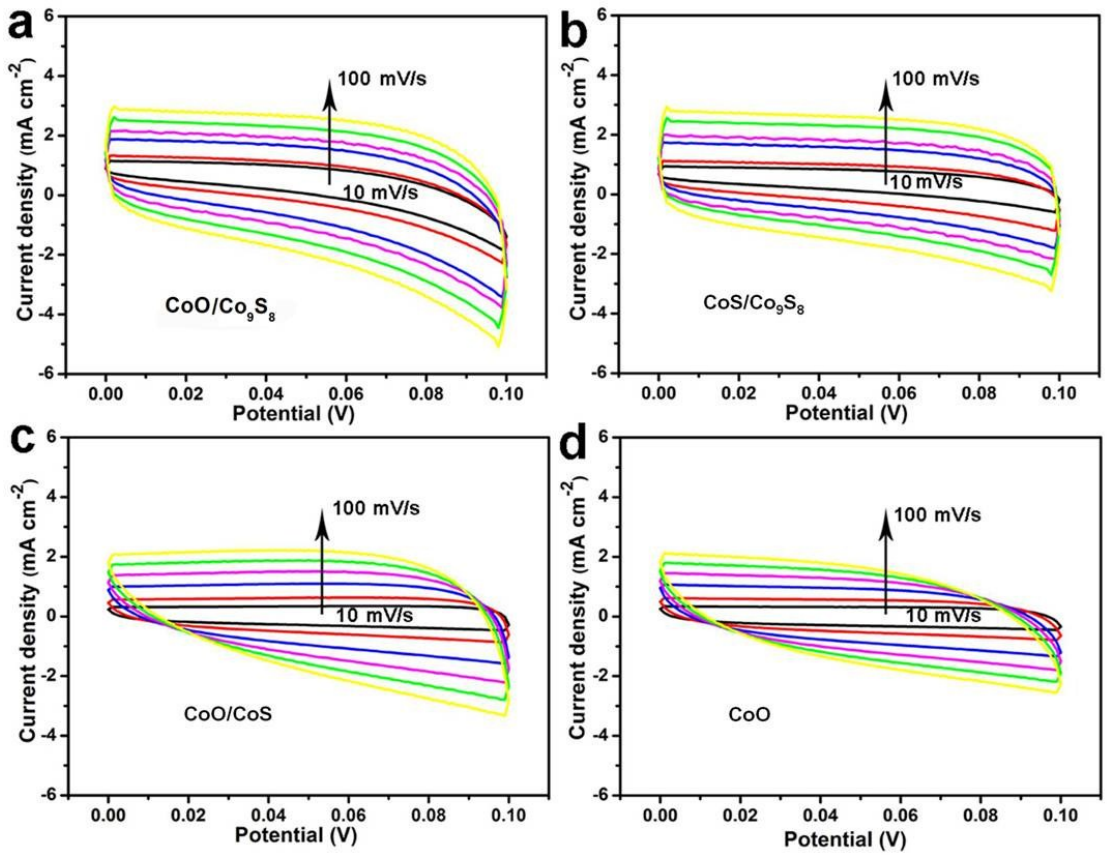

Fig. S11. CV curves of multi-shelled cobalt oxides/sulfides hollow microspheres within a non-Faradaic potential window (vs. SCE) at different scan rates. (a) CoO/Co_9S_8, (b) CoS/Co_9S_8, (c) CoO/CoS, (d) CoO.

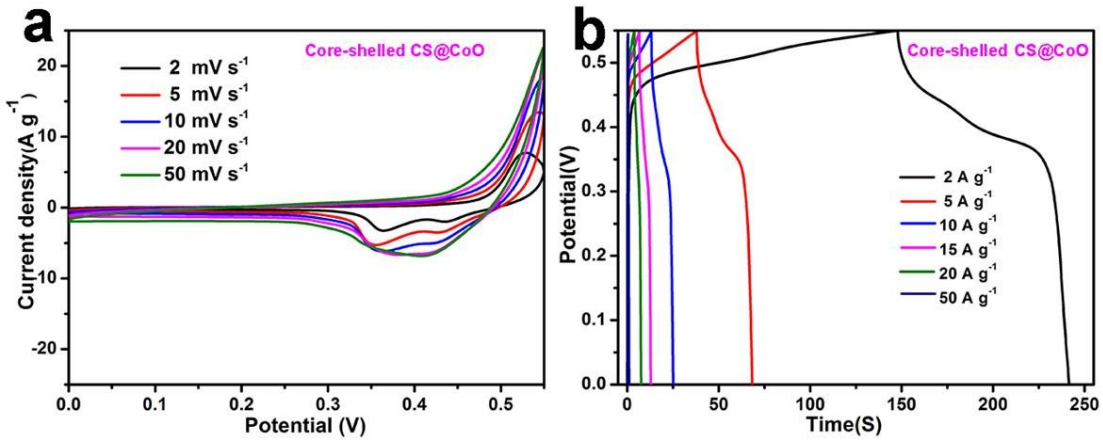

Fig. S12. CV curves performed at different scan rates (a) and GCCD curves at different current densities (b) of the CS@CoO microspheres.

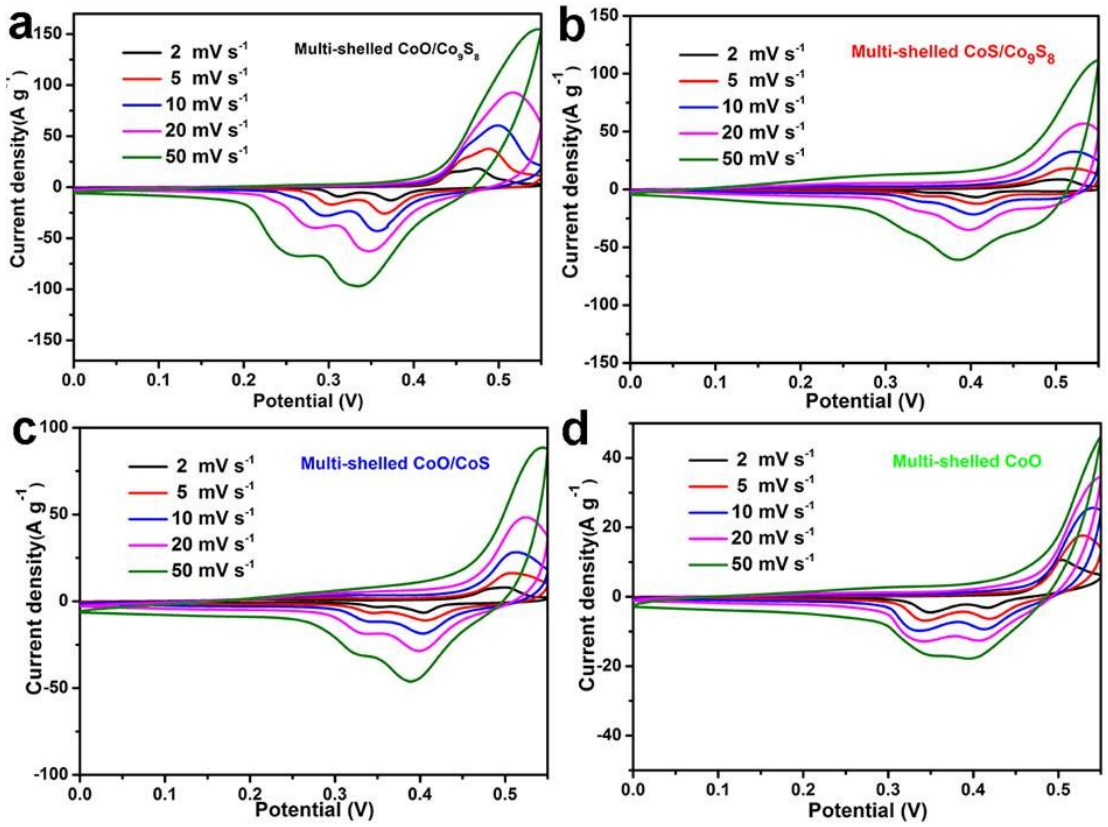

Fig. S13. CV curves performed at different scan rates of the multi-shelled cobalt oxides/sulfides composite hollow microspheres. (a) Co_9S_8/CoO, (b) CoS/Co_9S_8, (c) CoO/CoS, (d) CoO.

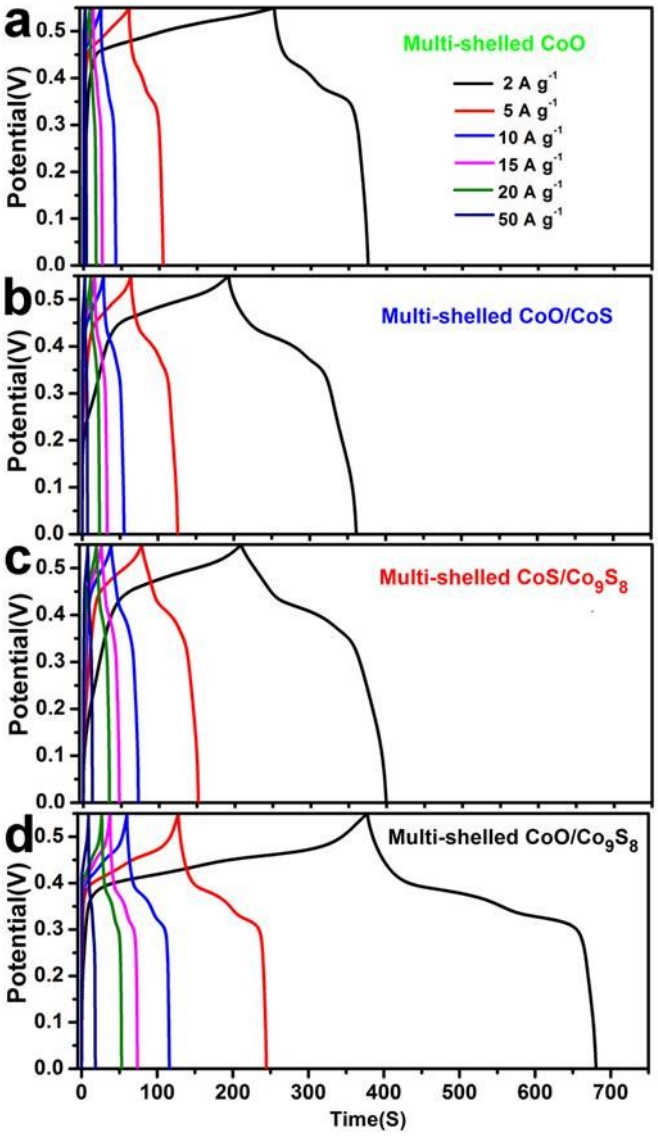

Fig. S14. GCCD curves performed at different current densities of the multi-shelled cobalt oxides/sulfides composite hollow microspheres. (a) CoO, (b) CoO/CoS, (c) CoS/Co_9S_8, (d) CoO/ Co_9S_8.

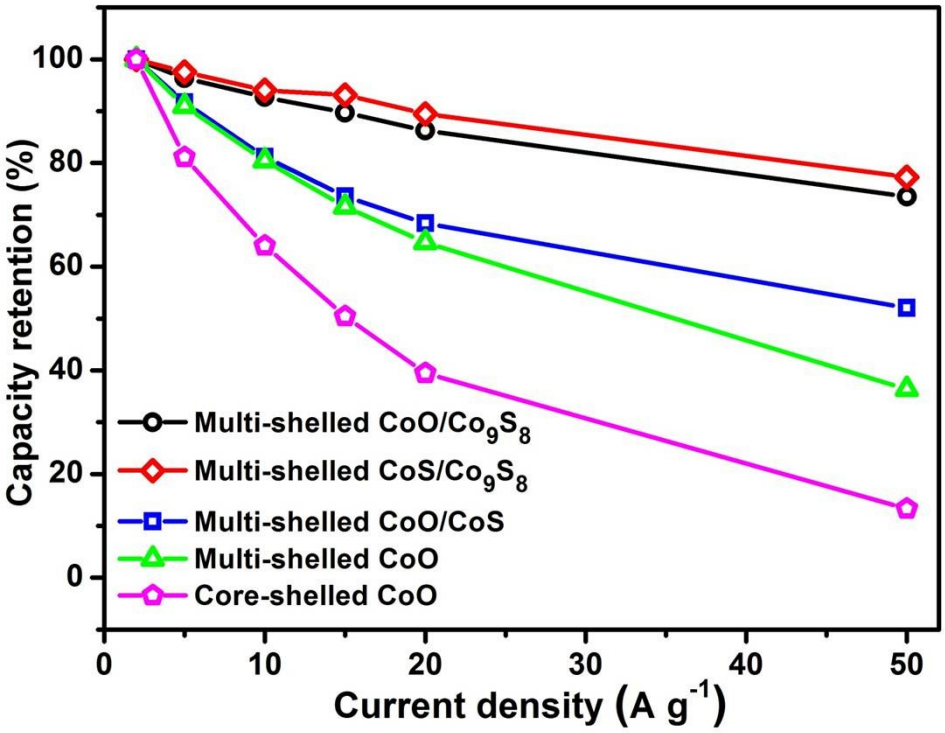

Fig. S15. The capacity retention at different current densities of the four multi-shelled cobalt oxides/sulfides composite hollow microspheres and CS@CoO microspheres.

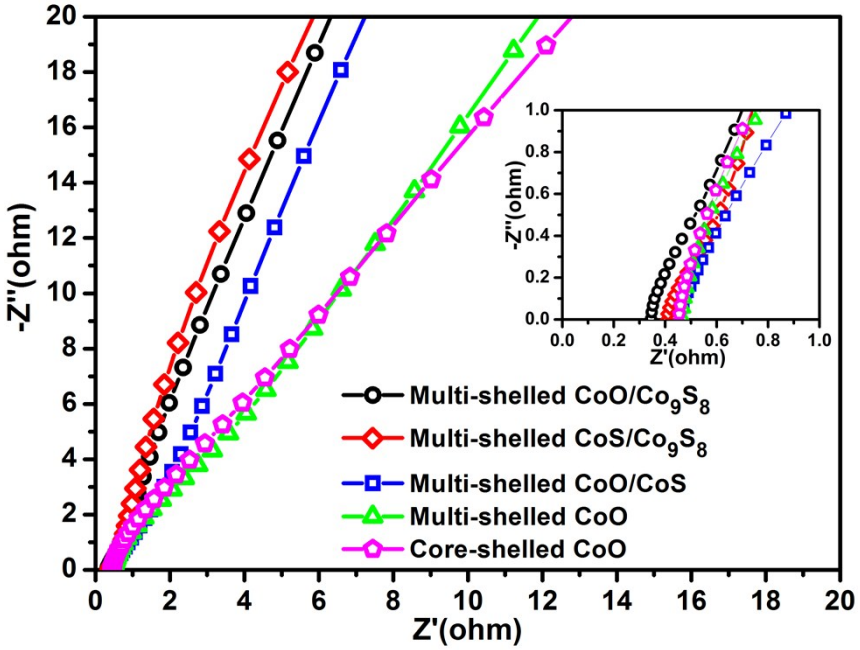

Fig. S16. Nyquist plots of theelectrochemical impedance spectroscopy (EIS) spectra for four multi-shelled cobalt oxides/sulfides composite hollow microspheres and CS@CoO microspheres.

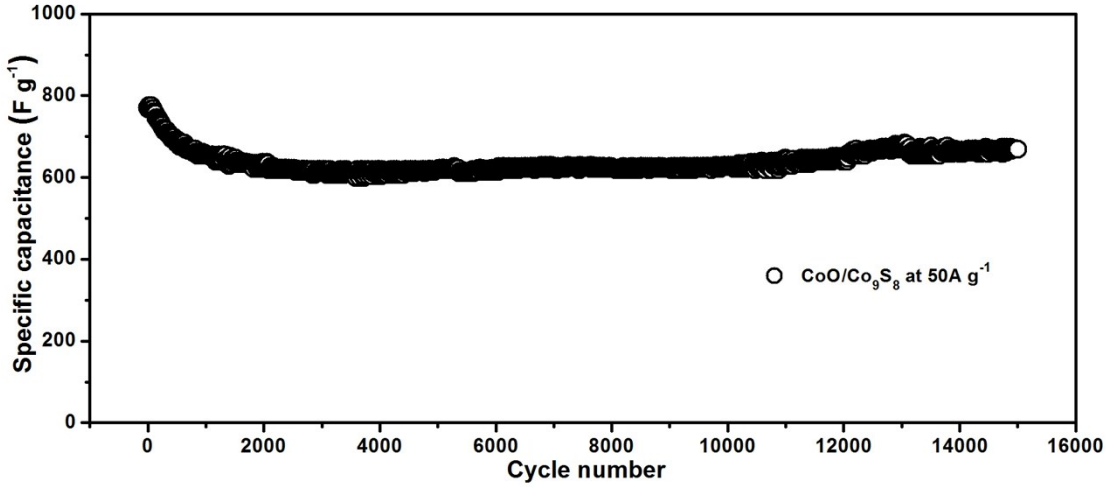

Fig. S17. Long-term cycling performance of multi-shelled CoO/Co_9S_8 at 50 A g^{-1}.

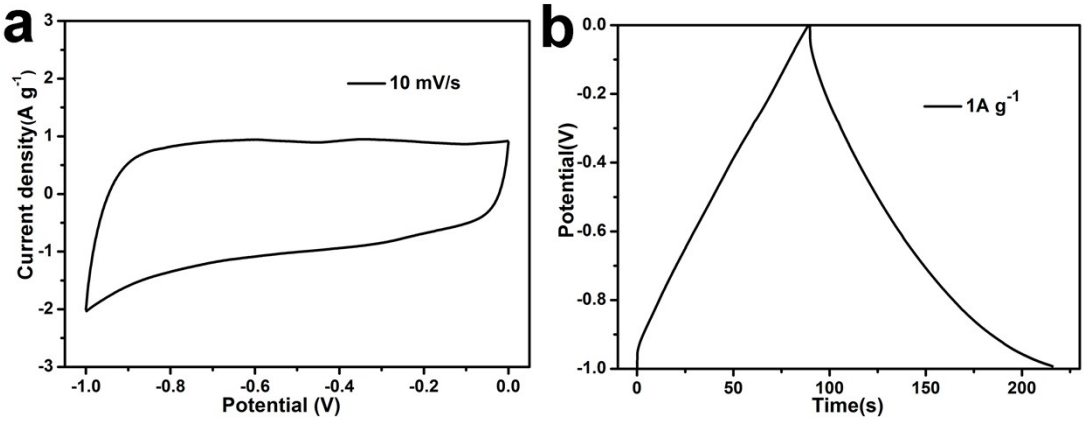

Fig. S18. The CV curve of the AC electrode at 10 mV s^{-1} (a) and the galvanostatic charge–discharge curve of the AC electrode at a current of 1 A g^{-1} (b).